NVP-AUY922: A Novel Heat Shock Protein 90 Inhibitor Active against Xenograft Tumor Growth, Angiogenesis, and Metastasis

Suzanne A. Eccles,[1] Andy Massey,[3] Florence I. Raynaud,[1] Swee Y. Sharp,[1] Gary Box,[1] Melanie Valenti,[1] Lisa Patterson,[1] Alexis de Haven Brandon,[1] Sharon Gowan,[1] Frances Boxall,[1] Wynne Aherne,[1] Martin Rowlands,[1] Angela Hayes,[1] Vanessa Martins,[1] Frederique Urban,[1] Kathy Boxall,[1] Chrisostomos Prodromou,[2] Laurence Pearl,[2] Karen James,[1] Thomas P. Matthews,[1] Kwai-Ming Cheung,[1] Andrew Kalusa,[1] Keith Jones,[1] Edward McDonald,[1] Xavier Barril,[3] Paul A. Brough,[3] Julie E. Cansfield,[3] Brian Dymock,[3] Martin J. Drysdale,[3] Harry Finch,[3] Rob Howes,[3] Roderick E. Hubbard,[3] Alan Surgenor,[3] Paul Webb,[3] Mike Wood,[3] Lisa Wright,[3] and Paul Workman[1]

[1]Cancer Research UK Centre for Cancer Therapeutics, The Institute of Cancer Research, Sutton, Surrey, United Kingdom; [2]Section of Structural Biology, The Institute of Cancer Research, Chester Beatty Laboratories, London, United Kingdom; and [3]Vernalis Ltd., Cambridge, United Kingdom

Abstract

We describe the biological properties of NVP-AUY922, a novel resorcinylic isoxazole amide heat shock protein 90 (HSP90) inhibitor. NVP-AUY922 potently inhibits HSP90 (K_d = 1.7 nmol/L) and proliferation of human tumor cells with GI_{50} values of approximately 2 to 40 nmol/L, inducing G_1-G_2 arrest and apoptosis. Activity is independent of NQO1/DT-diaphorase, maintained in drug-resistant cells and under hypoxic conditions. The molecular signature of HSP90 inhibition, comprising induced HSP72 and depleted client proteins, was readily demonstrable. NVP-AUY922 was glucuronidated less than previously described isoxazoles, yielding higher drug levels in human cancer cells and xenografts. Daily dosing of NVP-AUY922 (50 mg/kg i.p. or i.v.) to athymic mice generated peak tumor levels at least 100-fold above cellular GI_{50}. This produced statistically significant growth inhibition and/or regressions in human tumor xenografts with diverse oncogenic profiles: BT474 breast tumor treated/control, 21%; A2780 ovarian, 11%; U87MG glioblastoma, 7%; PC3 prostate, 37%; and WM266.4 melanoma, 31%. Therapeutic effects were concordant with changes in pharmacodynamic markers, including induction of HSP72 and depletion of ERBB2, CRAF, cyclin-dependent kinase 4, phospho-AKT/total AKT, and hypoxia-inducible factor-1α, determined by Western blot, electrochemiluminescent immunoassay, or immunohistochemistry. NVP-AUY922 also significantly inhibited tumor cell chemotaxis/invasion *in vitro*, WM266.4 melanoma lung metastases, and lymphatic metastases from orthotopically implanted PC3LN3 prostate carcinoma. NVP-AUY922 inhibited proliferation, chemomigration, and tubular differentiation of human endothelial cells and antiangiogenic activity was reflected in reduced microvessel density in tumor xenografts. Collectively, the data show that NVP-AUY922 is a potent, novel inhibitor of HSP90, acting via several processes (cytostasis, apoptosis, invasion, and angiogenesis) to inhibit tumor growth and metastasis. NVP-AUY922 has entered phase I clinical trials. [Cancer Res 2008;68(8):2850–60]

Introduction

The molecular chaperone heat shock protein 90 (HSP90) is an exciting target in oncology (1–3). It supports the correct conformation, stabilization, activation, and localization of "client" proteins, many of which are involved in tumor progression (4). Targeting several pathways is essential to prevent tumor cell "escape" and development of drug resistance (3). The therapeutic efficacy of HSP90 inhibitors probably relates to the combinatorial blockade of multiple signaling pathways (3, 5, 6) and the increased levels of active HSP90 in tumors (7, 8), in some cases linked to clinical outcome (9). Tumors may also become addicted to pathways dependent on activated, mutated, or overexpressed client proteins, the mutated forms of which (e.g., BRAF) are often hypersensitive to HSP90 inhibitors (10, 11). Thus, for a variety of reasons, inhibition of HSP90 has considerable clinical potential.

The geldanamycin class of HSP90 inhibitors has been extensively evaluated. Geldanamycin analogues, specifically 17-allylamino-17-demethoxygeldanamycin (17-AAG; tanespimycin), 17-(dimethylaminoethyl-amino)-17-demethoxygeldanamycin (17-DMAG; alvespimycin), and the 17-AAG hydroquinone IPI-504, have been developed as less toxic and/or more soluble drugs (12, 13). 17-AAG and 17-DMAG have been in several phase I and II clinical trials where some disease stabilization and tumor responses were seen (14–16). However, this compound series has limitations, including formulation difficulties, hepatotoxicity, variable pharmacokinetics, and polymorphic metabolism by CYP3A4 (17) and NQO1/DT-diaphorase enzymes (18), together with efflux by P-glycoprotein (18). Nevertheless, these agents have been invaluable for showing proof of principle of therapeutic benefit preclinically and clinically, for establishing and validating robust biomarkers of target modulation (14, 19, 20), and for identifying additional activities, including inhibition of tumor invasion (21, 22) and angiogenesis (23, 24).

Other natural product HSP90 inhibitors include the macrolide radicicol and its derivatives (25). Radicicol is poorly soluble and inactive *in vivo*, although semisynthetic oxime derivatives have improved pharmacokinetics and exhibit antitumor activity (25).

Note: Supplementary data for this article are available at Cancer Research Online (http://cancerres.aacrjournals.org/).

Requests for reprints: Suzanne A. Eccles or Paul Workman, Cancer Research UK Centre for Cancer Therapeutics, The Institute of Cancer Research, Cotswold Road, Belmont, Sutton, Surrey SM2 5NG, United Kingdom. Phone: 44-20-8722-4301; Fax: 44-20-8722-4324; E-mail: Sue.Eccles@icr.ac.uk or Paul.Workman@icr.ac.uk.

doi:10.1158/0008-5472.CAN-07-5256

However, these have not entered clinical development, possibly due to reported ocular toxicity (26).

There has been considerable effort to design synthetic small-molecule inhibitors based on the X-ray crystal structure of HSP90. Purine scaffold derivatives (e.g., PU3) showed parenteral activity in human tumor xenografts and soluble analogues exhibited oral antitumor activity at relatively high doses (27, 28). An oral purine scaffold compound (BIIBO21) is in clinical trial (29).

A second class of synthetic HSP90 inhibitors is the pyrazole resorcinols (Fig. 1*A*), initially exemplified by CCT018159 (30–32). Subsequent structure-based design generated more potent resorcinylic pyrazole/isoxazole amide analogues (33, 34) and the significantly improved isoxazole resorcinol NVP-AUY922 (VER-52296). NVP-AUY922 is the most potent synthetic small-molecule HSP90 inhibitor yet described (35). We now report on the detailed *in vitro* activity and *in vivo* pharmacokinetic, pharmacodynamic, and efficacy profiles of NVP-AUY922 in a wide spectrum of human tumor cell lines and xenografts with different molecular pathologies and including orthotopic and metastatic models. These results support the selection of NVP-AUY922 for clinical development.

Materials and Methods

NVP-AUY922 synthesis, activity, and selectivity. NVP-AUY922 was synthesized as described (35). Its activity was assayed against HSP90α, HSP90β, GRP94, TRAP-1, HSP72, and topoisomerase II (31, 34). Profiling against a panel of kinases was carried out and screening against a panel of additional enzymes and receptors was performed at Cerep. X-ray crystallography, fluorescence polarization, and isothermal calorimetry were as described (35–37).

Cell proliferation and cell cycle progression. Unless otherwise stated, cell lines were from the American Type Culture Collection and grown in DMEM/10% FCS, 2 mmol/L glutamine, and nonessential amino acids in a humidified atmosphere of 5% CO_2 in air as described (Supplementary

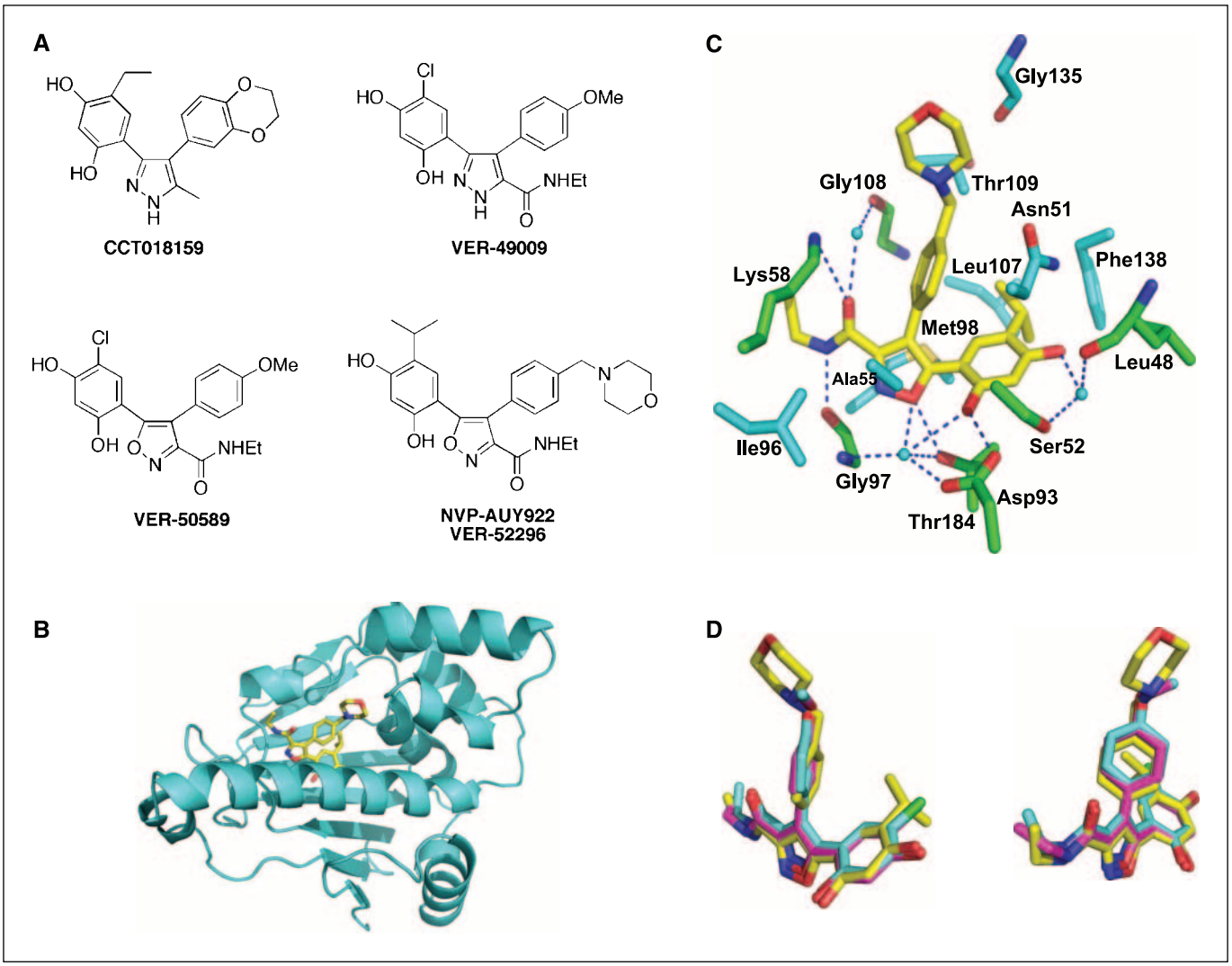

Figure 1. Chemical structures of resorcinylic isoxazole/pyrazole HSP90 inhibitors and X-ray cocrystal structures. *A,* chemical structures of the 3,4 diarylpyrazole/isoxazole resorcinol HSP90 inhibitors. *B,* PyMOL cartoon showing NVP-AUY922 bound to the NH_2-terminal domain of HSP90α. *C,* PyMOL diagram showing binding interactions of NVP-AUY922. *Dotted blue lines,* hydrogen bonds; *green,* amino acid residues involved; *cyan-colored spheres,* water molecules; *cyan,* residues solely in van der Waals contact. *D,* two orthogonal views of the superimposition of VER-49009 (*cyan*), VER-50589 (*magenta*), and NVP-AUY922 (*yellow*) showing that NVP-AUY922, VER-49009, and VER-50589 bind with overall similarity. The structures for NVP-AUY922, VER-50589, and VER-49009 were obtained at 2.0 Å, 2.0 Å, and 2.1 Å resolution, respectively. For atomic coordinates and structure factors, see PDB codes 2CVI, 2UWD, and 2BSM, respectively.

information; refs. 23, 31, 34). All lines were free of *Mycoplasma* (Venor GeM kit, Minerva Biolabs). Cell proliferation was determined using the sulforhodamine B (SRB) assay (18) for tumor cells and prostate epithelial cells, the WST-1 assay (Roche Diagnostics Ltd.) for MCF10A and HB119, or an alkaline phosphatase assay (23) for HUVEC and HDMEC. GI_{50} was the compound concentration inhibiting cell proliferation by 50% compared with vehicle controls. Cell cycle analysis was as described (31). Active caspase-3/7 was measured using a homogenous caspase assay kit (Promega).

Molecular biomarkers and tumor cell and endothelial cell activities. Effects of NVP-AUY922 on the expression of client proteins [e.g., CRAF, BRAF, cyclin-dependent kinase 4 (CDK4), ERBB2, AKT, and vascular endothelial growth factor receptor 2 (VEGFR2)] and on induction of HSP72 were determined in human tumor and endothelial cells (31, 34). Tumor cell chemotaxis, haptotaxis, invasion, and endothelial cell functions related to angiogenesis were also determined as described (23) with minor variations (see figure legends).

Measurement of NVP-AUY922 in biological samples. Microsomal incubations were performed with mouse and human liver preparations and human carcinoma cell uptake studies were as described (34). Given the relatively low GI_{50} for NVP-AUY922 in HCT116 colon carcinoma cells, we used $5 \times GI_{50}$ for cell uptake studies and equimolar concentrations in HT29 cells.

Xenograft pharmacokinetic and efficacy studies. *In vivo* pharmacokinetic studies in female NCr athymic mice bearing WM266.4 human melanoma xenografts were essentially as described (34). NVP-AUY922 was dissolved in DMSO and diluted in sterile saline/Tween 20. A single dose of 50 mg/kg NVP-AUY922 was given i.v. or i.p. and groups of three animals were taken at intervals for pharmacokinetic analyses. Further details are in Supplementary information.

For efficacy studies, human tumor xenografts were established s.c. in athymic mice. WM266.4 cells were also injected i.v. to generate experimental lung metastases and PC3LN3 prostate carcinoma cells were implanted into the prostates of male mice. Dosing with NVP-AUY922 commenced when tumors were well established using schedules described. Tumor growth was monitored and at study end samples were harvested for analysis. Further details are provided in Supplementary information.

Biomarker analyses by Western blotting, immunoassay, and immunohistochemistry. Snap-frozen tumors were lysed, protein concentration was determined, and standard Western blotting procedures were followed (34). The levels of phospho-AKT and/or total AKT, HSP72, ERBB2, extracellular signal-regulated kinase 1/2 (ERK1/2), and hypoxia-inducible factor-1α (HIF-1α) in treated and control tumor xenografts were determined by electrochemiluminescent immunoassay (Meso Scale Discovery).

Cryopreserved tumors were sectioned and stained for phosphoproteins. Details are in Supplementary information. Tumor microvessel density was determined as described (23).

Results

NVP-AUY922 binds to the NH_2-terminal nucleotide site in HSP90. The X-ray cocrystal structure of NVP-AUY922 (Fig. 1*A*) bound to the NH_2-terminal domain of recombinant human HSP90α is shown in Fig. 1*B* and *C*. This confirms the crucial network of hydrogen bonding interactions involving the resorcinol residue and heterocyclic ring with Asp^{93}, Thr^{184}, and a cluster of structurally conserved and highly ordered water molecules, as for CCT018159, VER-49009, and VER-50589 (31, 33, 34). In addition, as observed with VER-49009 and VER-50589, the C-5 ethylamide residue of NVP-AUY922 provides additional hydrogen bonding interactions with the protein backbone via Lys^{58} and Gly^{97}, the latter being particularly important (33). Replacement of the chlorine of the resorcinol ring in VER-49009 or VER-50589 by an isopropyl group in NVP-AUY922 results in an additional hydrophobic interaction with Leu^{107} in the flexible lipophilic pocket (Fig. 1*C*). Further hydrophobic interactions are also seen with Thr^{109} and Gly^{135} when the methoxy group of VER-49009 or VER-50589 is replaced with the morpholino moiety of NVP-AUY922. The morpholine ring is located close to the surface of the protein (Fig. 1*B*). The two orthogonal views of the superimposition of VER-49009, VER-50589, and NVP-AUY922 show that all three compounds bind with overall similarity (Fig. 1*D*).

NVP-AUY922 is a potent and selective HSP90 inhibitor. The competitive binding fluorescence polarization assay gave an IC_{50} for NVP-AUY922 of 21 ± 16 nmol/L against HSP90β (35) and of 7.8 ± 1.8 nmol/L for HSP90α. Inhibitory kinetics were competitive and the K_i values were 9.0 ± 5.0 nmol/L and 8.2 ± 0.7 nmol/L for HSP90α and HSP90β, respectively (mean ± SE, $n = 3$). Isothermal calorimetry showed a very high binding affinity to HSP90β with a K_d of 1.7 ± 0.5 nmol/L, 3-fold lower than VER-50589 (34). The enthalpy of binding of NVP-AUY922 is −12.24 kcal/mol, ~3 kcal/mol more favorable than for VER-50589 (34). The entropy of binding of NVP-AUY922 is almost negligible (0.19 cal/mol/K), indicating that the binding event is driven essentially exclusively by enthalpy (i.e., bonding interactions). NVP-AUY922 exhibits the tightest binding of any small-molecule HSP90 ligand yet reported.

The IC_{50} values for NVP-AUY922 against the HSP90 family members GRP94 and TRAP-1 were 535 ± 51 nmol/L (K_i = 108 nmol/L) and 85 ± 8 nmol/L (K_i = 53 nmol/L), respectively, indicating weaker potency than for HSP90. The fluorescence polarization IC_{50} for binding to HSP90 in human cell lysates was in the range of 6.0 ± 1.8 to 13.7 ± 1.4 with no clear differences between tumor cells (HCT116 and WM266.4) and nontumorigenic cells (HUVEC and PNT2 prostate epithelial cells). NVP-AUY922 at 10 μmol/L showed no inhibition of human HSP72 ATPase or the decatenation activity of human topoisomerase II and little or no activity against a range of 13 kinases (Supplementary Table S1). In a screen of 14 additional enzymes and 67 receptors, NVP-AUY922 exhibited >50% inhibitory activity at 10 μmol/L against only 6 receptors and 1 enzyme; further profiling showed NVP-AUY922 to be >50-fold selective for HSP90 (data not shown).

NVP-AUY922 potently inhibits proliferation of multiple human tumor cell lines *in vitro*. NVP-AUY922 inhibited with nanomolar potency (2.3–49.6 nmol/L) the *in vitro* proliferation of human tumor cells selected for their different tissue origins and molecular features (Supplementary Table S2). Unlike the geldanamycin-based HSP90 inhibitor 17-AAG (18, 38), NVP-AUY922 activity is independent of NQO1/DT-diaphorase activity because sensitivity was similar in BEneg human colon carcinoma cells carrying an inactivating *NQO1* polymorphism and isogenic BE2 cells transfected with the *NQO1* gene and also in SKMEL2 (high NQO1) and SKMEL5 (low NQO1) melanoma cells. Activity was maintained in doxorubicin-resistant CH1 ovarian carcinoma cells overexpressing P-glycoprotein and in oxaliplatin-resistant HT29 colon carcinoma cells. In addition, unlike some cytotoxic agents and radiotherapy, NVP-AUY922 was equally effective under hypoxic conditions. In PC3 and DU145 prostate carcinoma cells exposed to NVP-AUY922 in 20% or 1% O_2, the ratios of GI_{50} values were 1.17 and 1.20, respectively, whereas for paclitaxel the GI_{50} values were increased by 3.8- and 5.6-fold under hypoxia (data not shown). Nontumorigenic human prostate (PNT2 and Pre2.8) and breast (MCF10A and HB119) epithelial cells, at least when actively proliferating, showed similar sensitivity to NVP-AUY922 as tumor cells, as also seen with 17-AAG. Human endothelial cells (HUVEC and HDMEC) were among the most sensitive (Supplementary Table S2).

NVP-AUY922 induced marked accumulation in either G_1 or G_1 plus G_2-M phases in most cell lines. More detailed analysis using continuous bromodeoxyuridine (BrdUrd) labeling and

bivariate Hoechst-propidium iodide flow cytometry showed that NVP-AUY922 arrested HCT116 colon carcinoma cells in the original G_1 and G_2-M as early as 8 h (Fig. 2*A*). By 16 h, cells in S phase that had traversed to the new G_2* phase remained blocked over 72 h. The ability of NVP-AUY922 to induce apoptosis was cell line dependent. Activated caspase-3/7 levels rapidly increased in BT474 cells following exposure to NVP-AUY922 and apoptosis was confirmed by Western blotting for cleaved poly(ADP-ribose) polymerase (data not shown). In WM266.4 melanoma cells, activated caspase-3/7 increased moderately, whereas in MDA-MB-231 breast carcinoma and HCT116 colon carcinoma cells no increase was observed (Fig. 2*B*). Further analysis revealed that cell death could occur independently of caspase activation. Following 72-h exposure to 6 to 8 × GI_{50} concentrations of NVP-AUY922, the fraction of either BT474 or MDA-MB-231 breast carcinoma cells remaining was approximately 15% to 18% of pretreatment levels (Fig. 2*C*). In contrast, exposure of HCT116 colon carcinoma cells to 8 × GI_{50} NVP-AUY922 resulted in virtually no cell death, suggesting a predominantly cytostatic effect in this cell line.

These observations were confirmed by colony formation assays. The concentration of NVP-AUY922 required to reduce colony numbers to <1% following 24-h exposure was ~32 nmol/L for MDA-MB-231 cells but 250 nmol/L in HCT116 cells. This is not due to lack of client protein depletion as exposure of HCT116 cells to 5 × GI_{50} NVP-AUY922 led to a rapid depletion of CRAF and ERBB2 and concomitant induction of HSP72 (Fig. 2*D*). Despite being extremely sensitive to growth inhibition by NVP-AUY922, SKBR3 breast carcinoma cells also underwent cytostasis following exposure to NVP-AUY922 or 17-AAG (data not shown).

NVP-AUY922 shows high uptake in HCT116 human colon carcinoma cell lines *in vitro*. HT29 colon carcinoma cells express uridine diphosphoglucuronosyltransferases, whereas HCT116 cells do not (31, 39). At equimolar concentrations, initially high uptake was seen in both cell lines; however, ~3-fold more NVP-AUY922 was detected in HCT116 colon carcinoma cells following 1-h exposure (547.7 ± 4.5 pmol/10 million cells in HCT116 versus 172.0 ± 10.0 in HT29). Levels increased from 1 to 24 h to 687.0 ± 1.7 pmol/10 million cells in HCT116 cells but were hardly detectable at 24 h in HT29 cells (4.2 ± 0.8 pmol/10 million cells). This suggests that glucuronidation of NVP-AUY922 during this period results in the reduced sensitivity in HT29 cells compared with HCT116 cells.

NVP-AUY922 depletes HSP90 client proteins in a concentration- and time-dependent manner. The molecular signature of HSP90 inhibition comprises induction of HSP72 coupled with depletion of client proteins in a concentration- and time-dependent manner (14, 19). Biomarker changes were observed in HCT116 colon carcinoma cells (Fig. 2*D*) and in A2780 ovarian, SKMEL2 and WM266.4 melanoma, and BT474 breast carcinoma cells (Supplementary Fig. S1*A–D*). HSP72 levels were increased from 8 to 72 h. ERBB2 was almost completely depleted in all cell lines for the duration of the study. BRAF (both wild-type and

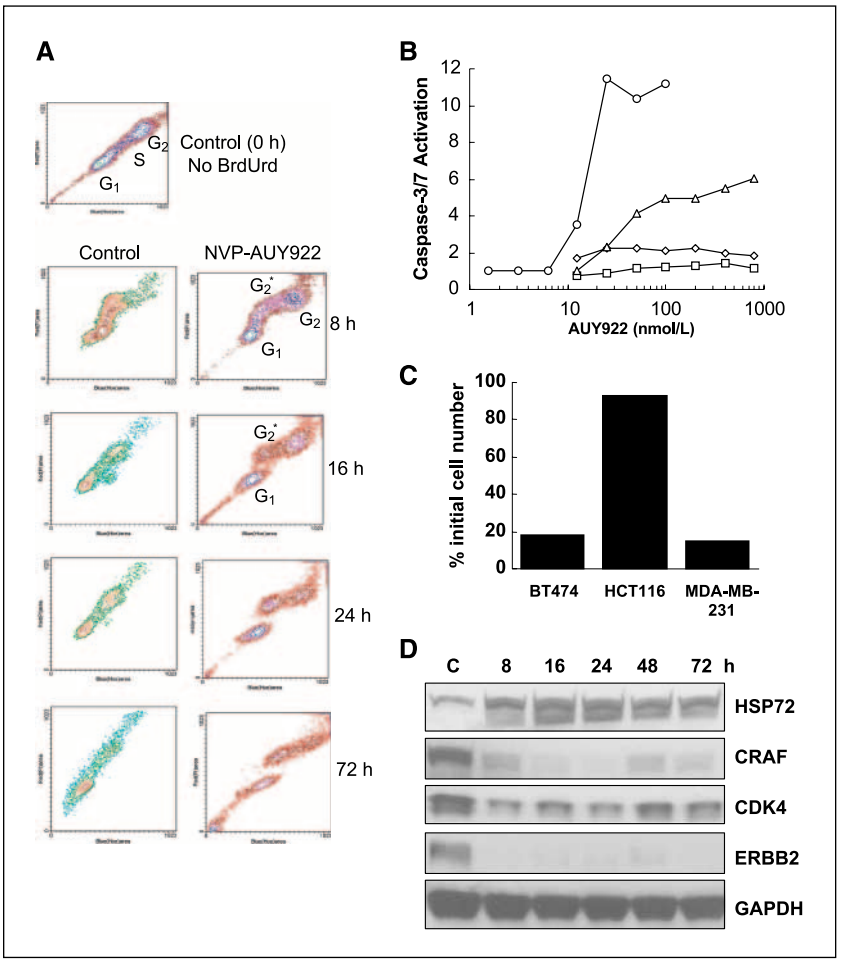

Figure 2. NVP-AUY922 induces cell cycle arrest and apoptosis and depletes client proteins in human cancer cells *in vitro*. *A,* representative cell cycle profiles of mutant *KRAS* HCT116 human colon carcinoma cells treated with vehicle (*left*) or 80 nmol/L (5 × GI_{50}) concentration of NVP-AUY922 (*right*) for 0, 8, 16, 24, and 72 h determined using continuous BrdUrd labeling and bivariate Hoechst-propidium iodide flow cytometry. *B,* BT474 breast carcinoma (*circles*), WM266.4 melanoma (*triangles*), MDA-MB-231 breast carcinoma (*diamonds*), or HCT116 colon carcinoma cells (*squares*) were exposed to increasing concentrations of NVP-AUY922 for 24 h. The amount of active caspase-3/7 was determined using a homogenous caspase assay kit. *C,* SRB determination of cell survival following exposure to NVP-AUY922 of BT474 (16 nmol/L), HCT116 (125 nmol/L), or MDA-MB-231 (40 nmol/L) cells for 72 h. Cell survival was determined as the percentage of cell mass remaining compared with that present at the start of NVP-AUY922 dosing. *D,* Western blot of HCT116 cells treated with 80 nmol/L (5 × GI_{50}) NVP-AUY922 and analyzed over 72 h. *GAPDH,* glyceraldehyde-3-phosphate dehydrogenase.

mutant forms in the SKMEL2 and WM266.4 cells, respectively) and CRAF were also depleted by NVP-AUY922 treatment. CDK4 levels showed cell-dependent responses (as previously noted with other HSP90 inhibitors) with decreased expression in most cell lines except WM266.4 and recovery evident between 72 and 96 h (Supplementary Fig. S1*A*; Fig. 2*D*).

Analysis of two key signaling events in BT474 breast carcinoma cells (phosphorylation of ERBB2 Tyr^{1240} and AKT Ser^{345}) indicated that NVP-AUY922 inhibited pathway activation at lower concentrations than those required to induce complete client protein depletion (Supplementary Fig. S2*A*). In SKBR3 breast carcinoma cells treated for 24 h with 4 × GI_{50} NVP-AUY922, ERBB2 was predominantly cytoplasmic rather than membrane bound as in control cells (Supplementary Fig. S2*B*).

NVP-AUY922 inhibits tumor cell chemomigration, invasion, and haptotaxis. Several HSP90 client proteins are implicated in cell motility and invasion (23, 24). Chemomigration of metastatic PC3LN3 prostate carcinoma cells in FluoroBlok assays was inhibited by 54% and 68% with 50 and 125 nmol/L (~2 × GI_{50} and 5 × GI_{50}) of NVP-AUY922. Similar effects were seen in Matrigel-coated filter invasion assays (Fig. 3*A*). In addition, in a scratch wound haptotaxis assay, PC3LN3 cells completed wound closure by 24 h, whereas cells exposed to 125 nmol/L NVP-AUY922 achieved only 60% closure at 48 h (Supplementary Fig. S4*A*). The rate of movement of PC3LN3 cells in the haptotaxis assay was also determined. Untreated cells moved on average 9.7 ± 1.1 μm/h and this rate was reduced to 56%, 40%, and 28% of controls by 50, 125, and 250 nmol/L of NVP-AUY922 (Supplementary Fig. S4*B*). WM266.4 melanoma cell migration and invasion were also very sensitive to NVP-AUY922: 50 nmol/L induced 90% and 78% inhibition, respectively (Supplementary Fig. S4*C*).

NVP-AUY922 inhibits endothelial cell functions related to angiogenesis *in vitro*. Human endothelial cells were highly sensitive to NVP-AUY922 in proliferation assays (GI_{50} = 2.5–3.9 nmol/L). In addition, HUVEC migration was inhibited in a concentration-dependent manner following 24-h exposure to NVP-AUY922 (Fig. 3*B*). At ~1 × GI_{50} concentrations (5 nmol/L), FCS-mediated chemomigration was reduced to 68% of controls, decreasing to 24% at 25 nmol/L. VEGF-driven HUVEC migration was even more sensitive: concentrations as low as 1 nmol/L inhibited chemotaxis by 50%, with complete inhibition at 2.5 nmol/L and above (Fig. 3*C*). HUVEC haptotaxis in a wound closure assay was also inhibited (data not shown). NVP-AUY922 inhibited HUVEC tubular differentiation on Matrigel in a concentration-dependent manner, with >80% inhibition at 25 nmol/L (Fig. 3*D*). We confirmed that HSP72 was induced and key angiogenic client proteins (including AKT and VEGFR2) were depleted concordantly, as measured by electrochemiluminescent immunoassay (Supplementary Fig. S3*A*–*C*) and Western blotting (Supplementary Fig. S3*D*).

NVP-AUY922 shows limited metabolism and favorable pharmacokinetics. Incubation of 10 μmol/L NVP-AUY922 with mouse and human liver microsomes for 30 min resulted in 69 ± 4% and 59 ± 15% metabolism (mean ± SE, n = 3), respectively, considerably less than the isoxazole VER-50589, which showed 71 ± 5% metabolism at 5 min and complete metabolism after 15 min of incubation (34). The main NVP-AUY922 metabolites measured in mouse plasma were the glucuronide of the parent, a deethylated product, and an oxidation product. The glucuronide represented ~95% of plasma metabolites as estimated by their area under the curves following i.v. and i.p. administration.

Plasma pharmacokinetic variables compared well with those described for other pyrazole and isoxazole HSP90 inhibitors (31, 34), with similar fast clearances following both i.p. and i.v. administration to athymic mice bearing WM266.4 human melanomas (Fig. 4*A*–*D*). However, as predicted from its decreased metabolism and high cellular uptake, NVP-AUY922 showed enhanced tissue distribution with ratios of ≥4.0 in WM266.4 tumors, liver, and spleen compared with plasma following i.v. administration. Importantly, tumor clearance was significantly lower than that of normal tissues, with a longer terminal half-life of 14.7 to 15.5 h. This resulted in tumor NVP-AUY922 levels at least 100 × GI_{50} concentrations over 24 h following both i.v. and i.p. administration. Similar pharmacokinetic profiles were observed in other human tumor xenografts as indicated below.

NVP-AUY922 inhibits HSP90 and exhibits potent antitumor efficacy in human tumor xenografts. Following five daily i.p. doses of 50 mg/kg NVP-AUY922 to athymic mice bearing *BRAF* mutant WM266.4 melanoma xenografts, liquid chromatography-tandem mass spectrometry analysis indicated NVP-AUY922 concentrations of 6.8 to 7.7 μmol/L in tumors over 24 h (Supplementary Table S3). As quantified by electrochemiluminescent immunoassay, ERBB2 levels were reduced to a nadir of 7.3% of controls at 6 h, remaining below 35% over 24 h. Phospho-ERK1/2 levels were 65% to 83%, phospho-AKT levels were 13% to 51%, AKT levels were 57% to 65%, and HIF-1α levels were 60% to 85%. HSP72 expression was increased to 247% to 281% of controls over the 24-h period.

The therapeutic effect of NVP-AUY922 was determined against established WM266.4 melanoma xenografts. Daily doses of 75 mg/kg caused ~10% body weight loss; thus, doses were reduced to 50 mg/kg/d after eight doses and body weights rapidly recovered. NVP-AUY922 significantly inhibited tumor growth rate, reducing the mean weights of tumors on day 11 from 252 ± 19 mg in controls to 78 ± 6 mg (Fig. 5*A*). Tumor samples on day 11 (24 h after the final dose) showed the HSP90 inhibition signature of depleted ERBB2 and CDK4, with induced HSP72 (Fig. 5*B*).

We next tested 50 mg/kg NVP-AUY922 given i.p. or i.v. daily against established WM266.4 melanoma xenografts. The treatment regimens were well tolerated with either no (i.p.) or <5% (i.v.) differences in mean body weights compared with controls. Tumor weights after 9 days of treatment were reduced by 55% in the i.v. group (P = 0.000085) and by 46% in the i.p. group (P = 0.00067) compared with controls. Biomarker changes confirmed HSP90 inhibition in tumor as in the previous study. Both routes of administration gave comparable levels of NVP-AUY922 in the tumors (similar to those reported above in the single dose studies), consistent with the comparable efficacy and pharmacodynamic changes observed. In three additional studies, mice with established WM266.4 tumors were treated with different schedules of NVP-AUY922, and in all cases, significant growth delays were observed, with some recovery of growth rate toward the end of dosing (Supplementary Table S5).

We also tested the ability of NVP-AUY922 to inhibit established disseminated melanoma. Therapy commenced 7 days after i.v. injection of WM266.4 melanoma cells and continued for 32 days (50 mg/kg five times weekly for 18 days, three times weekly for a further 14 days). Histologic examination of lungs indicated that both the number and size of lung metastases were decreased by NVP-AUY922 treatment (Fig. 5*C*). The mean number of metastases was reduced from 61 ± 13 to 17 ± 3 (72% inhibition; P = 0.0037) and the total area occupied by the metastases decreased from

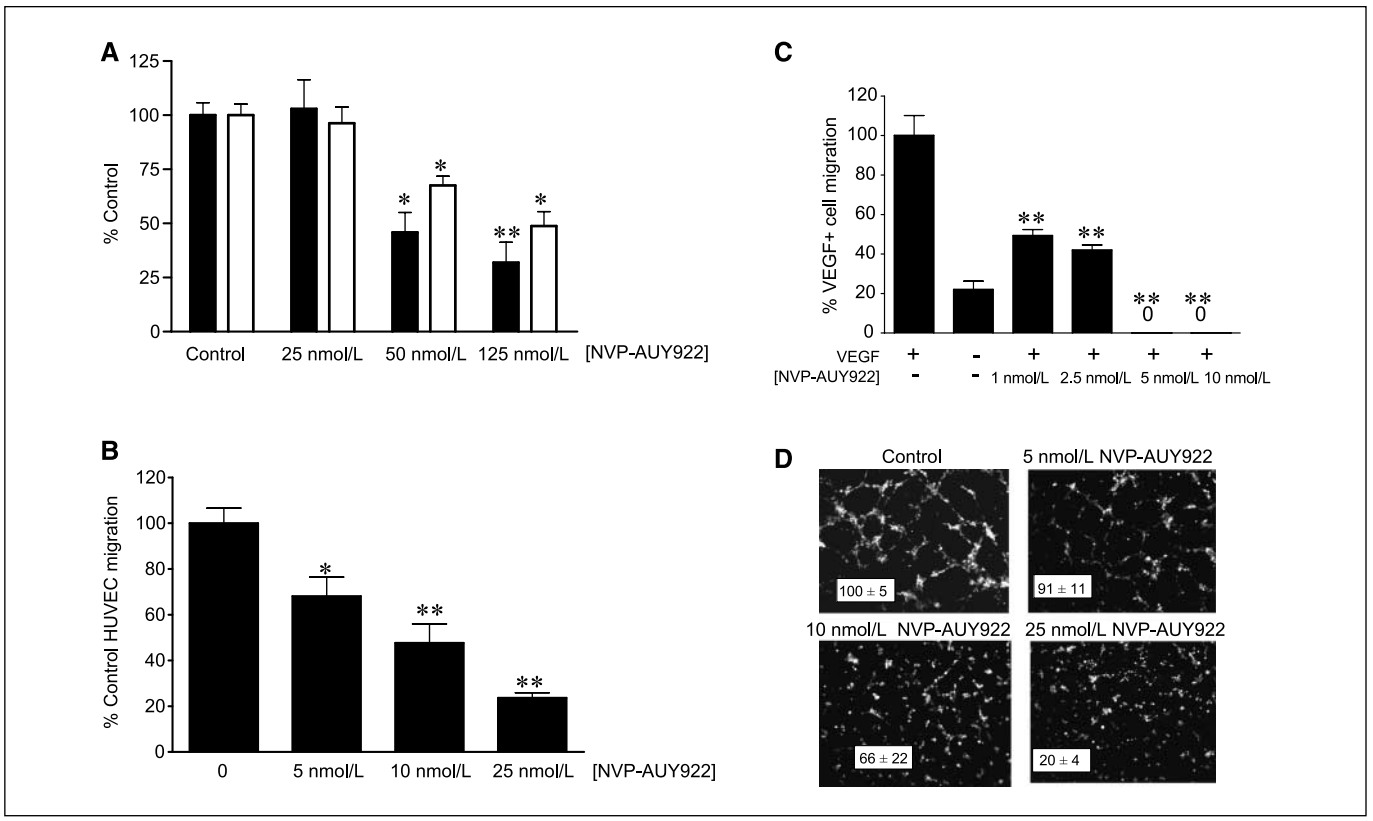

Figure 3. NVP-AUY922 potently inhibits tumor cell and endothelial cell functions *in vitro*. PTEN-null PC3LN3 human prostate carcinoma or human endothelial cells (HUVEC) were treated with NVP-AUY922 or vehicle at various concentrations for 24 h before being tested for their ability to migrate through FluoroBlok filters (8- and 3-μm pore sizes, respectively) in response to chemoattractants as described in Materials and Methods. Invasion was measured using Matrigel-coated filters (BD Biosciences). *A,* PC3LN3 migration (*black columns*) and invasion (*white columns*) toward 5% FCS; NVP-AUY922 concentrations tested represent approximately 1 to 5 × GI_{50}. The migration assay was terminated after 16 h and the invasion assay after 36 h. *, $P \leq 0.05$; **, $P < 0.001$, relative to control cell migration to FCS. *B,* HUVEC migration toward 5% FCS; NVP-AUY922 concentrations tested represent approximately 1 to 5 × GI_{50}. The assay was terminated after 3 h. *C,* HUVEC migration in response to 50 ng/mL VEGF (+) or in the absence of VEGF (−), the latter representing background motility. Cells stimulated with VEGF were treated with increasing concentrations of NVP-AUY922. The filters were precoated with collagen 1 to aid HUVEC attachment. The assay was terminated after 16 h. *, $P \leq 0.05$; **, $P < 0.001$, relative to control VEGF-stimulated cell migration. *D,* HUVECs, which had been pretreated with NVP-AUY922 for 24 h, were plated onto Matrigel in six-well plates and incubated at 37°C for 6 h to determine their ability to undergo tubular differentiation. Representative images are shown together with quantitation of tubule area (% of area of control cultures) determined by Image-Pro Plus software.

2.38 ± 0.43 mm^2 to 0.15 ± 0.04 mm^2 (93.7% inhibition; $P = 0.0003$) as shown in Fig. 5*D*.

We then determined the efficacy of NVP-AUY922 in established PTEN-null U87MG human glioblastoma xenografts. Again, highly significant growth inhibition was obtained; indeed, regressions were observed because mean tumor volumes on day 18 were decreased to 58% of day 0 values (Fig. 6*A*). HSP90 inhibition was confirmed by Western blot with significant depletion of ERBB2, AKT, phospho-ERK1/2, HIF-1α, and survivin together with increased HSP72 (data not shown). We also showed clear depletion of phospho-AKT (Ser^{473}) and phospho-S6 ($Ser^{240/244}$) in histologic sections, consistent with inhibition of the phosphatidylinositol 3-kinase (PI3K) pathway (Fig. 6*B*). Figure 6*C* shows that levels of HIF-1α and AKT were decreased to 39% and 27% of controls, respectively, and HSP72 levels increased by ~800% as measured by electrochemiluminescent immunoassay. Finally, microvessel density was significantly reduced in NVP-AUY922–treated tumors, suggesting an antiangiogenic effect (Fig. 6*D*).

A parallel pharmacokinetic/pharmacodynamic study of five daily doses (50 mg/kg i.p., comparable with that described above for WM266.4) was performed in U87MG xenografts. Mean tumor NVP-AUY922 concentrations were 3.8 to 6.7 μmol/L from 6 to 24 h following the last dose (Supplementary Table S4). Phospho-AKT expression was reduced to 19% to 56%, AKT to 74% to 80%, and HIF-1α to 32% to 48% of controls over 6 to 24 h. Phospho-ERK1/2 levels were apparently not decreased in this tumor but HSP72 expression was increased to 228% to 530% of controls (data not shown).

The therapeutic efficacy of NVP-AUY922 was explored in further human tumor xenografts of varying histogenic origins and with differing molecular abnormalities. Strong inhibitory effects were obtained in the *PTEN* and *PIK3CA* mutant A2780 ovarian carcinoma [treated/control (T/C) of 10.5% after 8 daily treatments with 50 mg/kg i.p.; Supplementary Fig. S5*A*] and the $ERBB2^+$ $ER\alpha^+$ BT474 breast carcinoma (T/C of 21% after 24 daily treatments; Supplementary Fig. S5*B*). In the latter case, regressions were observed in 5 of 12 tumors. Body weight loss was <5% and clear biomarker changes consistent with HSP90 inhibition were obtained in both studies (Supplementary Fig. S5*C* and *D*). In BT474, complete loss of ERBB2 and substantial depletion of ERα were shown, in addition to reductions in CDK4 and phospho-ERK1/2.

Finally, we explored the ability of NVP-AUY922 (50 mg/kg daily i.p.) to inhibit growth and spontaneous metastasis in an established orthotopic and metastatic PTEN-null human prostate

carcinoma xenograft model (PC3LN3). Primary tumor growth was reduced (Supplementary Fig. S6*A*), as was the incidence and mass of local lymph node metastases (Supplementary Fig. S6*B*). Fifty-three percent of control animals developed distant lymph node metastases, but none was detected in the NVP-AUY922–treated animals. Western blots showed induction of HSP72, strong depletion of ERBB2, and weak but detectable depletion of CDK4 (Supplementary Fig. S6*C*). The antitumor activity of NVP-AUY922 in all human tumor xenograft models tested is summarized in Supplementary Table S5.

Discussion

NVP-AUY922 was discovered in a multiparameter lead optimization program (35) based on a high-throughput screening hit (30). Initial activities focused on improving potency against the HSP90 target using X-ray crystallography and structure-based drug design, resulting in the resorcinol pyrazole amide VER-49009 (31, 33). Replacement of the pyrazole with isoxazole led to VER-50589 with further increments in target affinity and enhanced cellular uptake and antiproliferative activity with acceptable pharmacokinetic-pharmacodynamic properties, leading to antitumor activity in HCT116 xenografts (34). Further lead optimization, focussing on maintaining or increasing potency while improving physicochemical properties and pharmacokinetic-pharmacodynamic behavior, resulted in NVP-AUY922 (35).

To our knowledge, NVP-AUY922 exhibits the highest affinity of any synthetic small-molecule inhibitor yet reported for the NH_2-terminal nucleotide-binding site of human HSP90, with a K_d of 1.7 $\pm$ 0.5 nmol/L. The binding potency is explained by the bonding

A

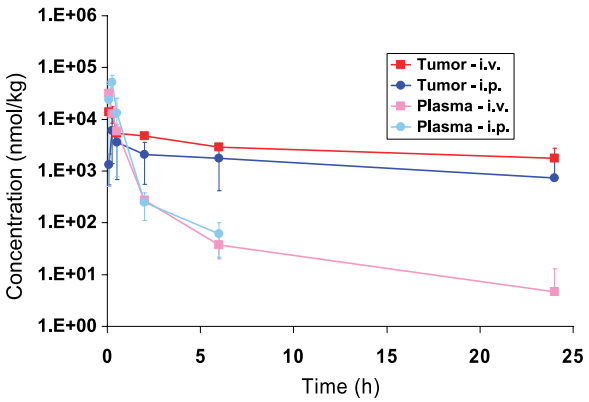

B

	Route	Tmax (h)	Cmax (nmol/L)	AUClast (h*nmol/L)	HL_Lambda_z (h)	Vss_obs (L)	Cl_obs (L/h)	AUCINF_obs (h*nmol/L)	Vz_obs (L)
Plasma	i.v.	-	48936	15009	4.243	0.090	0.143	15038	0.875
	i.p.	0.25	52506	26254	0.655	-	0.082	26311	0.077
Tumor	i.v.	0.08	13907	70027	15.462	-	0.020	109114	0.440
	i.p.	0.25	6078	36126	14.746	-	0.041	51834	0.883

C

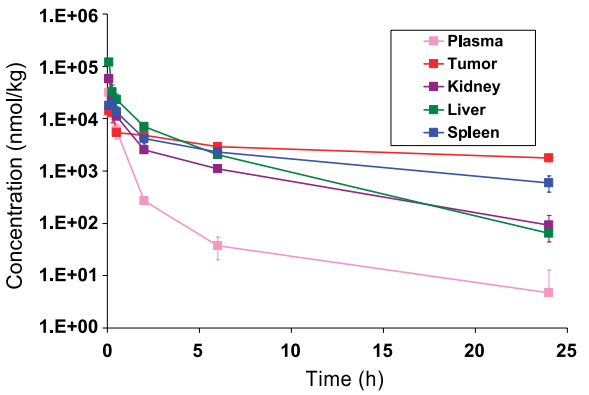

D

Tissue	Tmax (h)	Cmax (nmol/L)	AUClast (h*nmol/L)	HL_Lambda_z (h)	Vss_obs (L)	Cl_obs (L/h)	AUCINF_obs (h*nmol/L)	Vz_obs (L)	Tissue:Plasma (AUClast ratio)
Plasma	-	48936	15009	4.2	0.090	0.143	15038	0.875	-
Tumor	0.08	13907	70027	15.5	-	0.020	109114	0.440	4.7
Kidney	0.25	24786	35943	4.7	-	0.059	36575	0.402	2.4
Liver	0.08	118667	84018	3.4	-	0.026	84329	0.123	5.6
Spleen	0.25	19625	60605	8.2	-	0.032	67701	0.377	4.0

Figure 4. NVP-AUY922 achieves therapeutic concentrations in human tumor xenografts in athymic mice. Concentration versus time course and pharmacokinetic parameters for NVP-AUY922 following a single dose of 50 mg/kg i.v. or i.p. to mice bearing *BRAF* mutant WM266.4 human melanoma xenografts. *A,* plasma and tumor levels following i.v. or i.p. administration. *B,* pharmacokinetic parameters comparing i.v. and i.p. routes. *C,* plasma, tumor, and normal tissue levels following i.v. administration. *D,* pharmacokinetic parameters following i.v. administration. *Points,* mean of three animals; *bars,* SD.

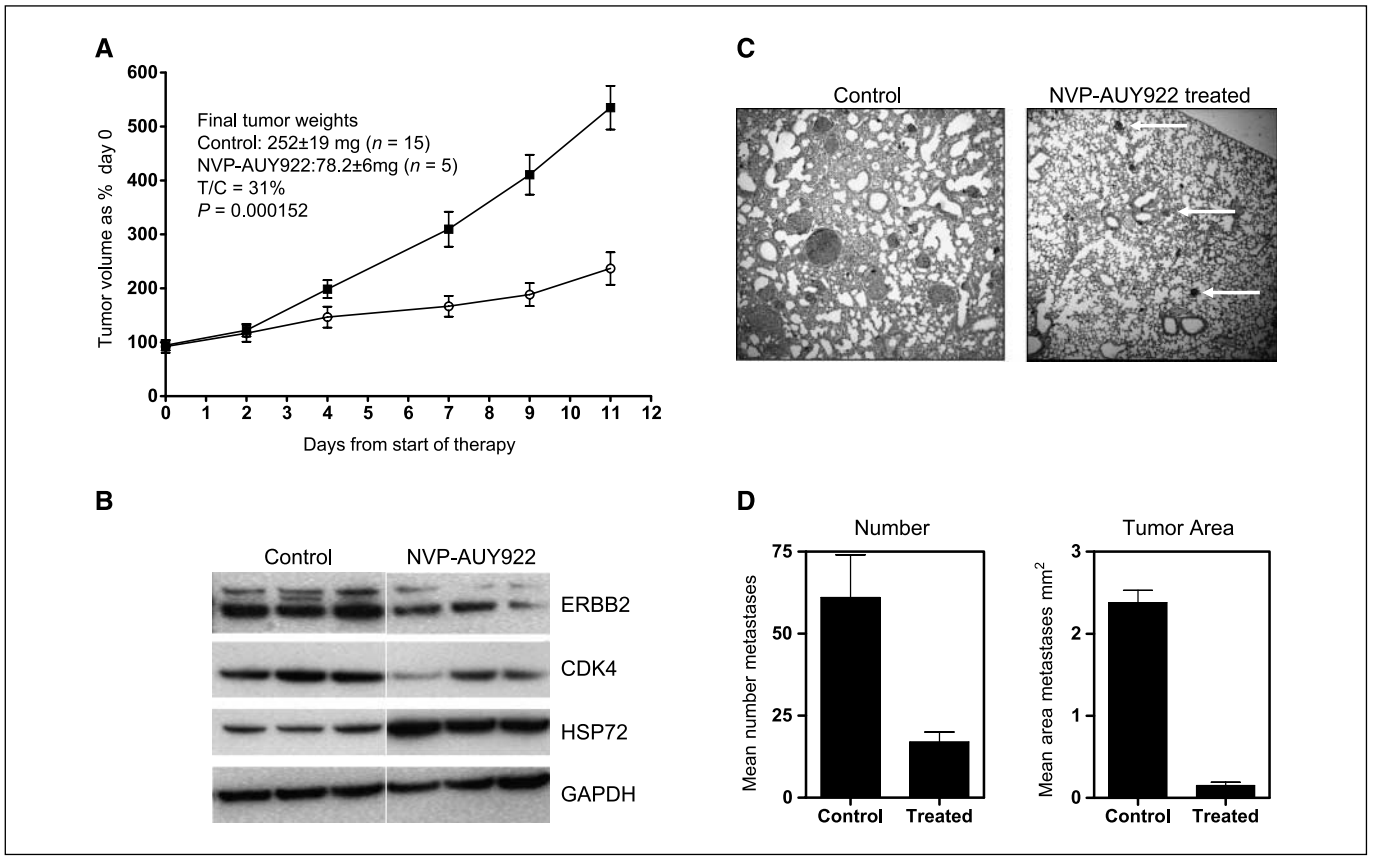

Figure 5. NVP-AUY922 shows therapeutic activity against established *BRAF* mutant WM266.4 human melanoma xenografts and lung metastases. Xenografts of the $BRAF^{V600D}$ mutant WM266.4 human melanoma were established s.c. bilaterally in the flanks of female NCr athymic mice as described in Supplementary Materials and Methods. Groups of animals were randomized to vehicle or drug treatment when the mean tumor diameter was 5 to 6 mm (day 8 after tumor cell implantation). Animals initially received 75 mg/kg NVP-AUY922 (or an equivalent volume of vehicle) i.p. daily for eight doses, and then the dose was reduced to 50 mg/kg until day 11 when samples were obtained for analyses (24 h following the final dose). Results are expressed as % of tumor volumes at the commencement of therapy. In a second study, WM266.4 cells were injected i.v. to model lung metastases. Therapy with NVP-AUY922 was initiated 7 d later and continued five times weekly for 18 d and then three times weekly for a further 14 d. Lungs were excised, weighed, and sectioned, and lung metastases were scored by image analysis of three random fields of view per lung in sections taken at three different depths. *A,* xenograft tumor growth curves, with final weights and other metrics (*inset*). ■, vehicle controls; ○, NVP-AUY922 treated. *B,* Western blots of three representative control and three NVP-AUY922–treated xenografts (day 11) showing expression levels of molecular pharmacodynamic biomarkers 24 h after the final dose. *C,* examples of WM266.4 lung colonies in control and NVP-AUY922–treated animals. *Left,* large tumors are evident in the lungs of control animals; *right, arrows,* examples of micrometastases in treated animals. *D,* quantitation of number and size of WM266.4 lung colonies in control and NVP-AUY922–treated mice.

interactions revealed by the X-ray cocrystal structure, together with the entropy and enthalpy factors. NVP-AUY922 also exhibited a degree of selectivity against the HSP90 target over the highly homologous HSP90 family members GRP94 and TRAP-1. This is distinct from 17-AAG, which exhibits moderate selectivity over GRP94 but is highly selective against TRAP-1. In addition, NVP-AUY922 at 10 μmol/L showed no significant inhibition of the related GHKL family member human topoisomerase II, was inactive against human HSP72, and exhibited little or no inhibition of a large panel of additional kinases, other enzymes, and receptors.

The human tumor cells sensitive to NVP-AUY922 represent diverse tissue origins and were selected to exhibit a range of key molecular abnormalities, including PTEN loss (e.g., PC3 and U87MG) and expression of activated oncogenes such as the *ERBB* family (e.g., BT474, SKBR3, T47D, and DU145), mutant *KRAS* (HCT116), mutant *PIK3CA* (HCT116, A2780, and BT474), mutant *BRAF* (WM266.4, SKMEL28, BE, and HT29), and mutant *TP53* (SKMEL2 and SKMEL28). The activity seen across the tumor cell line panel (Supplementary Table S2) suggests that NVP-AUY922 could have wide therapeutic applicability. Its cellular potency is significantly enhanced compared with earlier isoxazole and pyrazole resorcinols developed in this research program. Mean GI_{50} values in comparable tumor cell panels are as follows: NVP-AUY922, 10.8 nmol/L versus 5,300 nmol/L for CCT018159, 685 nmol/L for VER-49009, and 78 nmol/L for VER-50589, representing an ~5,000-fold improvement from the original hit and a 6.6-fold enhancement compared with the recently reported isoxazole VER-50589 (34). Importantly, NVP-AUY922 activity is independent of NQO1/DT-diaphorase metabolism, is equally effective in cells with acquired resistance to oxaliplatin or doxorubicin, and retains activity under hypoxic conditions.

In human HCT116 colon carcinoma cells and others, exposure to NVP-AUY922 resulted in G_1 and G_2-M arrest. However, this is cell line and tumor type dependent, as seen with other HSP90 inhibitors (31, 40), because G_1 arrest only was observed in SKMEL5 melanoma cells and BT474 breast cancer cells. There was clear evidence of concentration- and time-dependent biomarker modulation and induction of HSP72 expression, the accepted molecular signature of HSP90 inhibition (14, 19). At 5 × GI_{50} concentrations, client protein depletion was usually evident by 8 h, although CDK4 levels fell later and recovered sooner or in some cells were relatively unaffected. Inhibition of signaling (as evidenced by the loss of

phosphorylated ERBB2 and AKT in high ERBB2-expressing breast carcinoma cells) could often be detected before degradation of client protein. Previous reports have shown that depletion of key client proteins (such as ERBB2 and AKT) is closely correlated with antiproliferative effects of benzoquinone ansamycin HSP90 inhibitors and that the pharmacodynamic changes are generally seen at 4 to 5 × GI_{50} concentrations (14, 19). Our findings with NVP-AUY922, a member of a different chemical class of HSP90 inhibitor, are consistent with these observations.

Cell fate following HSP90 inhibition varied between cell lines and involved caspase-dependent or caspase-independent cell death or cytostasis. It is likely that the expression of factors downstream of loss of client protein signaling following HSP90 inhibition is critical for subsequent cell fate. Identification of factors that confer cell survival through induction of cell stasis rather than death may help to determine sensitive patient populations. The fact that inhibition of other cellular functions (such as chemomigration) occurs at concentrations below those required for cytostasis attests to their particular reliance on HSP90 chaperones (22).

In addition to the enhanced cellular potency of NVP-AUY922, further advantages were obtained from decreased microsomal metabolism, leading to reduced glucuronide metabolite in plasma compared with previously described pyrazoles and isoxazoles (32, 34). This translated into a significant improvement in tumor distribution. Indeed, NVP-AUY922 was selected from a set of similar compounds based on sustained high tumor levels following cassette dosing in tumor-bearing mice (35). Following i.v. and i.p. administration of 50 mg/kg NVP-AUY922, tumor levels were ~100 × GI_{50} and sustained for at least 24 h. Given the cellular accumulation observed with NVP-AUY922, it is likely that high concentrations are required in tumors for robust target inhibition and therapeutic efficacy. HSP90 is abundant in tumor cells. The concentration of 820 to 1,100 nmol NVP-AUY922/million cells measured in HCT116 following treatment with 5 × GI_{50} concentrations would correspond to ~5 μmol/L in tumor tissue based on protein measurements. These levels are within the concentration range observed following single and multiple dosing in animals (Fig. 4). Similar high levels were observed in human tumor xenograft models following 17-AAG treatment (19) and would be predicted to occur in cancers of treated patients based on plasma pharmacokinetics (14).

NVP-AUY922 was well tolerated in mice at 50 mg/kg/d and showed excellent target inhibition evidenced by depletion of multiple client proteins and induction of HSP72, leading to therapeutic efficacy in a wide variety of human tumor xenografts with different molecular pathologies. The results compare favorably with those for VER-50589 (34) and with other HSP90 inhibitors (29, 41). Significant

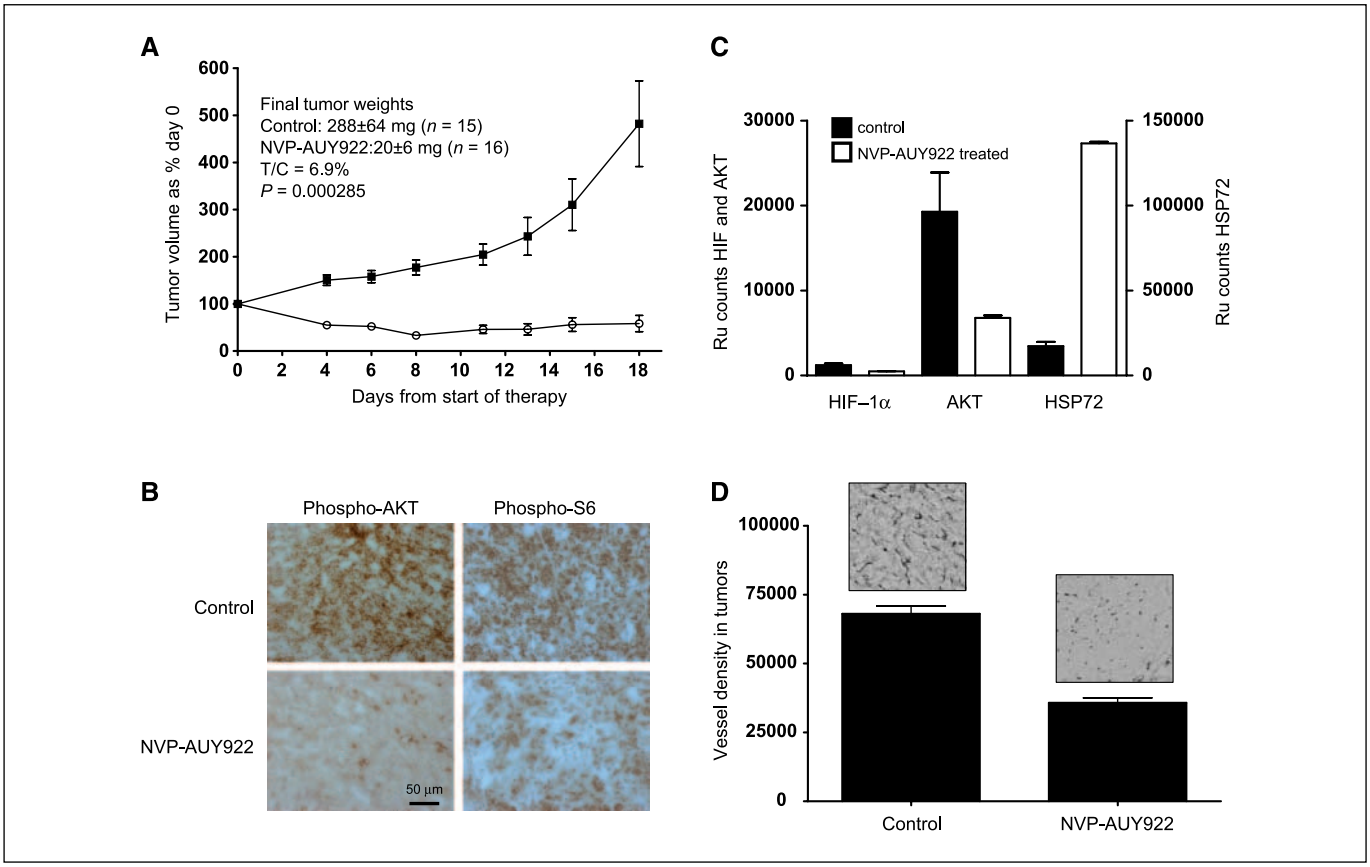

Figure 6. NVP-AUY922 shows therapeutic activity against established PTEN-null U87MG human glioblastoma xenografts. Tumors were established s.c. bilaterally in the flanks of female NCr athymic mice as described in Supplementary Materials and Methods. Groups of eight animals were randomized to vehicle or drug treatment when the mean tumor diameter was 5 to 6 mm (day 8 after tumor cell implantation). Animals received 50 mg/kg NVP-AUY922 i.p. five times weekly (or an equivalent volume of vehicle) for 18 d when the study was terminated and samples were obtained for analyses. Results are expressed as % of tumor volumes at the commencement of therapy. *A,* xenograft tumor growth curves, with final weights and other metrics (*inset*). ■, vehicle controls; ○, NVP-AUY922 treated. *B,* immunostaining for phospho-AKT and phospho-S6 in tumor xenografts. *C,* electrochemiluminescence immunoassay measuring tumor levels of HIF-1α, AKT, and HSP72. *D,* tumor microvessel density with representative images of vessel staining (*inset* above). *Left,* control; *right,* NVP-AUY922 treated. $P < 0.0001$, Student's *t* test.

tumor growth inhibition (T/C, 50%) was previously shown with NVP-AUY922 in HCT116 xenografts (35), and here, we extended these observations to established melanoma, glioblastoma, and breast, ovarian, and prostate carcinomas. In some tumors (e.g., BT474 breast cancer and U87MG glioblastoma), regressions were obtained. In all cases, robust therapeutic responses correlated with clear biomarker modulation and with compound levels in tumors well above the GI_{50} for sustained periods.

In addition to effects on s.c. human tumor xenografts, it is notable that mutant BRAF-expressing melanoma lung metastases were inhibited by NVP-AUY922 because ~70% of melanomas harbor such activating mutations (42) and there are no effective treatments for disseminated disease. Interestingly, in a phase I trial of 17-AAG, sustained responses were obtained in two melanoma patients with good biomarker responses (14). High levels of HSP90 have been reported in human melanomas compared with benign nevi, and fluorescence-activated cell sorting analysis of cells isolated from melanoma metastases indicated cell surface expression of HSP90 (43), reflecting experimental studies suggesting that a proportion of HSP90 is extracellular and associated with tumor cell invasion (21). Thus, malignant melanoma is an exciting target for NVP-AUY922 and other HSP90 inhibitors.

ERα and ERBB2 HSP90 client proteins were depleted in BT474 human breast cancer cells and tumor xenografts by NVP-AUY922, consistent with the therapeutic response seen in this model. Hence, there is optimism that patients with either hormone-responsive or hormone-nonresponsive breast carcinomas may obtain therapeutic benefit from HSP90 inhibitors. HSP90 is overexpressed in human breast cancer and expression correlates with survival (9). Of great interest is the recent report of responses to 17-AAG plus trastuzumab in patients with trastuzumab-refractory breast cancers (16). In addition, heregulin β1 (an ERBB ligand) induces HSP90, contributing to protection from apoptosis/anoikis (44). Thus, HSP90 inhibition should reverse this survival advantage and indeed 17-AAG sensitizes SKBR3 and BT474 breast carcinoma cells to proapoptotic stimulators such as paclitaxel (45). Similar results were obtained in ovarian carcinoma cells with high levels of activated AKT (46).

Prostate cancers, which may express androgen receptors or dependency on the PI3K pathway by virtue of PTEN deletion, may also respond well to HSP90 inhibitors. 17-AAG was reported to slow the growth of androgen-dependent and androgen-independent human prostate cancer xenografts at s.c. sites (47). Here, we show for the first time that a HSP90 inhibitor can limit the growth of established orthotopic PTEN-null, hormone-independent prostate carcinoma xenografts and can also block the development of spontaneous lymphatic metastases. Thus, hormone-independent prostate cancer is another example in which acceptable treatment options are limited and where NVP-AUY922 may have therapeutic potential.

HIF-1α is a HSP90 client protein in renal cell carcinoma cells where its high expression is due to loss of the von Hippel Lindau gene product (48). HIF-1α is also regulated by hypoxia, oncogenes, or activated receptor tyrosine kinases such as ERBB2, EGFR, and insulin-like growth factor-I receptor (49). Here, we show that NVP-AUY922 is equally active under hypoxic conditions and depletes HIF-1α in U87MG human glioblastoma tumor xenografts. Because HIF-1α is implicated in tumor angiogenesis, invasion, and drug resistance (49), this extends the potential of HSP90 inhibitors to target these key aspects of tumor progression. Indeed, we provide evidence that NVP-AUY922 potently inhibits tumor cell invasion, endothelial cell functions associated with angiogenesis *in vitro* (proliferation, motility, matrix invasion, and tubular differentiation), and tumor vascularization *in vivo*, as previously shown for 17-AAG and 17-DMAG (23, 24).

Geldanamycin and 17-AAG were reported to inhibit invasion of tumor cells *in vitro* (21, 22); however, these findings were not extended to *in vivo* therapy studies of invasion or metastasis. The present article provides, to our knowledge, the first evidence that a HSP90 inhibitor can inhibit both hematogenous and spontaneous lymphatic metastases in preclinical xenograft models. 17-AAG was shown to enhance bone metastasis in a breast carcinoma xenograft model (50). The inhibition of lung and lymphatic metastasis reported here suggests that these effects may be context and/or chemical class dependent.

Although 17-AAG has shown early promise as a first-in-class, proof-of-concept HSP90 inhibitor and is in phase II clinical trial, it has formulation issues and is associated with significant toxicity, such as liver dysfunction, optical neuritis, dyspnea, fatigue, and gastrointestinal side effects (14, 15). It is unclear which toxicities are associated specifically with HSP90 inhibitors (on-target effects) and which are related to specific chemical scaffolds [e.g., the benzoquinone moiety (off-target effects)]. There is therefore a need to discover and develop alternative inhibitors. NVP-AUY922 was derived from our resorcinylic pyrazole/isoxazole amide series (31, 33, 34) and is, to our knowledge, the most potent synthetic small-molecule inhibitor yet reported. In addition, optimization of pharmacokinetic-pharmacodynamic properties led to robust therapeutic responses in a wide variety of human tumor xenografts (including orthotopic and metastatic models) tightly linked to high intratumoral concentrations of compound and clear pharmacodynamic responses. Taken together, these data support the selection of NVP-AUY922 as an exciting candidate for clinical evaluation. NVP-AUY922 has entered phase I clinical trials.

Acknowledgments

Received 9/11/2007; revised 12/21/2007; accepted 1/14/2008.

Grant support: Cancer Research UK [CUK] programme grants CA309/A2187 and C309/A8274 (S.A. Eccles, F.I. Raynaud, S.Y. Sharp, G. Box, M. Valenti, L. Patterson, A. de Haven Brandon, S. Gowan, F. Boxall, W. Aherne, M. Rowlands, A. Hayes, V. Martins, F. Urban, K. Boxall, K. James, T.P. Matthews, K-M. Cheung, A. Kalusa, K. Jones, E. McDonald, and P. Workman), Wellcome Trust (C. Prodromou and L. Pearl), and Vernalis Ltd. (A. Massey, X. Barril, P.A. Brough, J.E. Cansfield, B. Dymock, M.J. Drysdale, H. Finch, R. Howes, R.E. Hubbard, A. Surgenor, P. Webb, M. Wood, and L. Wright). P. Workman is a Cancer Research UK Life Fellow.

The costs of publication of this article were defrayed in part by the payment of page charges. This article must therefore be hereby marked *advertisement* in accordance with 18 U.S.C. Section 1734 solely to indicate this fact.

References

1. Sharp S, Workman P. Inhibitors of the HSP90 molecular chaperone: current status. Adv Cancer Res 2006;95:323–8.
2. Whitesell L, Lindquist SL. HSP90 and the chaperoning of cancer. Nat Rev Cancer 2005;5:761–72.
3. Workman P, Burrows F, Neckers L, Rosen N. Drugging the cancer chaperone HSP90: combinatorial therapeutic exploitation of oncogene addiction and tumor stress. Ann N Y Acad Sci 2007;1113:202–16.
4. Pearl LH, Prodromou C. Structure and mechanism of the Hsp90 molecular chaperone machinery. Annu Rev Biochem 2006;75:271–94.
5. Chiosis G. Targeting chaperones in transformed systems—a focus on Hsp90 and cancer. Expert Opin Ther Targets 2006;10:37–50.
6. Xu W, Neckers L. Targeting the molecular chaperone heat shock protein 90 provides a multifaceted effect on diverse cell signalling pathways of cancer cells. Clin Cancer Res 2007;13:1625–9.

7. Kamal A, Thao L, Sensintaffar J, et al. A high-affinity conformation of Hsp90 confers tumour selectivity on Hsp90 inhibitors. Nature 2003;425:407–10.
8. Mosser DD, Morimoto RI. Molecular chaperones and the stress of oncogenesis. Oncogene 2004;23:2907–18.
9. Pick E, Kluger Y, Giltnane JM, et al. High HSP90 expression is associated with decreased survival in breast cancer. Cancer Res 2007;67:2932–7.
10. da Rocha Dias S, Friedlos F, Light Y, Springer C, Workman P, Marais R. Activated B-RAF is an Hsp90 client protein that is targeted by the anticancer drug 17-allylamino-17-demethoxygeldanamycin. Cancer Res 2005;65:10686–91.
11. Grbovic OM, Basso AD, Sawai A, et al. V600E B-Raf requires the Hsp90 chaperone for stability and is degraded in response to Hsp90 inhibitors. Proc Natl Acad Sci U S A 2006;103:57–62.
12. Ge J, Normant E, Porter JR, et al. Design, synthesis, and biological evaluation of hydroquinone derivatives of 17-amino-17-demethoxygeldanamycin as potent, water-soluble inhibitors of Hsp90. J Med Chem 2006; 49:4606–15.
13. Sausville EA, Tomaszewski JE, Ivy P. Clinical development of 17-allylamino, 17-demethoxygeldanamycin. Curr Cancer Drug Targets 2003;3:377–83.
14. Banerji U, O'Donnell A, Scurr M, et al. Phase I pharmacokinetic and pharmacodynamic study of 17-allylamino, 17-demethoxygeldanamycin in patients with advanced malignancies. J Clin Oncol 2005;23:4152–61.
15. Pacey S, Banerji U, Judson I, Workman P. Hsp90 inhibitors in the clinic. Handbook Exp Pharmacol 2006; 172:331–58.
16. Modi S, Stopeck AT, Gordon MS, et al. Combination of trastuzumab and tanespimycin (17-AAG, KOS-953) is safe and active in trastuzumab-refractory HER-2 overexpressing breast cancer: a phase I dose-escalation study. J Clin Oncol 2007;25:5410–7.
17. Egorin MJ, Rosen DM, Wolff JH, Callery PS, Musser SM, Eiseman JL. Metabolism of 17-(allylamino)-17-demethoxygeldanamycin (NSC 330507) by murine and human hepatic preparations. Cancer Res 1998;58:2385–96.
18. Kelland LR, Sharp SY, Rogers PM, Myers TG, Workman P. DT-diaphorase expression and tumor cell sensitivity to 17-allylamino, 17-demethoxygeldanamycin, an inhibitor of heat shock protein 90. J Natl Cancer Inst 1999;91:1940–9.
19. Banerji U, Walton M, Raynaud F, et al. Pharmacokinetic-pharmacodynamic relationships for the heat shock protein 90 molecular chaperone inhibitor 17-allylamino, 17-demethoxygeldanamycin in human ovarian cancer xenograft models. Clin Cancer Res 2005;11:7023–32.
20. Maloney A, Clarke PA, Naaby-Hansen S, et al. Gene and protein expression profiling of human ovarian cancer cells treated with the heat shock protein 90 inhibitor 17-allylamino-17-demethoxygeldanamycin. Cancer Res 2007;67:3239–53.
21. Eustace BK, Sakurai T, Stewart JK, et al. Functional proteomic screens reveal an essential extracellular role for hsp90α in cancer cell invasiveness. Nat Cell Biol 2004;6:507–14.
22. Xie Q, Gao CF, Shinomiya N, et al. Geldanamycins exquisitely inhibit HGF/SF-mediated tumor cell invasion. Oncogene 2005;24:3697–707.
23. Sanderson S, Valenti M, Gowan S, et al. Benzoquinone ansamycin heat shock protein 90 inhibitors modulate multiple functions required for tumor angiogenesis. Mol Cancer Ther 2006;5:522–32.
24. Kaur G, Belotti D, Burger AM, et al. Antiangiogenic properties of 17-(dimethylaminoethylamino)-17-demethoxygeldanamycin: an orally bioavailable heat shock protein 90 modulator. Clin Cancer Res 2004;10: 4813–21.
25. Agatsuma T, Ogawa H, Akasaka K, et al. Halohydrin and oxime derivatives of radicicol: synthesis and antitumor activities. Bioorg Med Chem 2002;10:3445–54.
26. Janin YL. Heat shock protein 90 inhibitors. A text book example of medicinal chemistry? J Med Chem 2005;48:7503–12.
27. Vilenchik M, Solit D, Basso A, et al. Targeting wide-range oncogenic transformation via PU24FCl, a specific inhibitor of tumor Hsp90. Chem Biol 2004;11:787–97.
28. Biamonte MA, Shi J, Hong K, et al. Orally active purine-based inhibitors of the heat shock protein 90. J Med Chem 2006;49:817–28.
29. Chiosis G, Lopes EC, Solit D. Heat shock protein 90 inhibitors: a chronicle from geldanamycin to today's agent. Curr Opin Invest Drugs 2006;7:534–41.
30. Cheung KM, Matthews TP, James K, et al. The identification, synthesis, protein crystal structure and *in vitro* biochemical evaluation of a new 3,4-diarylpyrazole class of Hsp90 inhibitors. Bioorg Med Chem Lett 2005;15:3338–43.
31. Sharp SY, Rowlands M, Prodromou CS, et al. *In vitro* biological characterization of a novel, synthetic diaryl pyrazole resorcinol class of HSP90 inhibitors. Cancer Res 2007;67:2206–16.
32. Smith NF, Hayes A, James K, et al. Preclinical pharmacokinetics and metabolism of a novel diaryl pyrazole resorcinol series of heat shock protein 90 inhibitors. Mol Cancer Ther 2006;5:1628–37.
33. Dymock BW, Barril X, Brough PA, et al. Novel, potent small-molecule inhibitors of the molecular chaperone Hsp90 discovered through structure-based design. J Med Chem 2005;48:4212–5.
34. Sharp SY, Clarke PA, Powers M, et al. Inhibition of the heat shock protein 90 molecular chaperone *in vitro* and *in vivo* by novel, synthetic, potent resorcinylic pyrazole/isoxazole amide analogues. Mol Cancer Ther 2007;6: 1198–211.
35. Brough PA, Aherne W, Barril X, et al. 4,5-Diarylisoxazole Hsp90 chaperone inhibitors: potential therapeutic agents for the treatment of cancer. J Med Chem 2008;51:196–218.
36. Howes R, Barril X, Dymock BW, et al. A fluorescence polarization assay for inhibitors of Hsp90. Anal Biochem 2006;350:202–13.
37. Roe SM, Prodromou C, O'Brien R, Ladbury JE, Piper PW, Pearl LH. Structural basis for inhibition of the Hsp90 molecular chaperone by the antitumor antibiotics radicicol and geldanamycin. J Med Chem 1999; 42:260–6.
38. Sharp SY, Kelland LR, Valenti MR, Brunton LA, Hobbs S, Workman P. Establishment of an isogenic human colon tumor model for NQO1 gene expression: application to investigate the role of DT-diaphorase in bioreductive drug activation *in vitro* and *in vivo*. Mol Pharmacol 2000;58:1146–55.
39. Cummings J, Zelcer N, Allen JD, et al. Glucuronidation as a mechanism of intrinsic drug resistance in colon cancer cells: contribution of drug transport proteins. Biochem Pharmacol 2004;67:31–9.
40. Hostein I, Robertson D, DiStefano F, Workman P, Clarke PA. Inhibition of signal transduction by the Hsp90 inhibitor 17-allylamino-17-demethoxygeldanamycin results in cytostasis and apoptosis. Cancer Res 2001; 61:4003–9.
41. Zhang L, Fan J, Vu K, et al. 7′-Substituted benzothiazolothio- and pyridinothiazolothio-purines as potent heat shock protein 90 inhibitors. J Med Chem 2006;49: 5352–62.
42. Davies H, Bignell GR, Cox C, et al. Mutations of the BRAF gene in human cancer. Nature 2002;417:949–54.
43. Becker B, Multhoff G, Farkas B, et al. Induction of Hsp90 protein expression in malignant melanomas and melanoma metastases. Exp Dermatol 2004;13:27–32.
44. Khaleque MA, Bharti A, Sawyer D, et al. Induction of heat shock proteins by heregulin β1 leads to protection from apoptosis and anchorage-independent growth. Oncogene 2005;24:6564–73.
45. Solit DB, Basso AD, Olshen AB, Scher HI, Rosen N. Inhibition of heat shock protein 90 function down-regulates Akt kinase and sensitizes tumors to Taxol. Cancer Res 2003;63:2139–44.
46. Sain N, Krishnan B, Ormerod MG, et al. Potentiation of paclitaxel activity by the HSP90 inhibitor 17-allylamino-17-demethoxygeldanamycin in human ovarian carcinoma cell lines with high levels of activated AKT. Mol Cancer Ther 2006;5:1197–208.
47. Solit DB, Zheng FF, Drobnjak M, et al. 17-Allylamino-17-demethoxygeldanamycin induces the degradation of androgen receptor and HER-2/neu and inhibits the growth of prostate cancer xenografts. Clin Cancer Res 2002;8:986–93.
48. Isaacs JS, Jung YJ, Mimnaugh EG, Martinez A, Cuttitta F, Neckers LM. Hsp90 regulates a von Hippel Lindau-independent hypoxia-inducible factor-1α-degradative pathway. J Biol Chem 2002;277:29936–44.
49. Bardos JI, Ashcroft M. Hypoxia-inducible factor-1 and oncogenic signalling. Bioessays 2004;26:262–9.
50. Price JT, Quinn JM, Sims NA, et al. The heat shock protein 90 inhibitor, 17-allylamino-17-demethoxygeldanamycin, enhances osteoclast formation and potentiates bone metastasis of a human breast cancer cell line. Cancer Res 2005;65:4929–38.

NVP-AUY922: A Novel Heat Shock Protein 90 Inhibitor Active against Xenograft Tumor Growth, Angiogenesis, and Metastasis

Suzanne A. Eccles, Andy Massey, Florence I. Raynaud, et al.

Cancer Res 2008;68:2850-2860.